Neuroscience 162 (2009) 1023–1038

Ca^{2+} ENTRY THROUGH A NON-SELECTIVE CATION CHANNEL IN *APLYSIA* BAG CELL NEURONS

J. E. GEIGER, C. M. HICKEY AND N. S. MAGOSKI*

Department of Physiology, Queen's University, 4th Floor, Botterell Hall, 18 Stuart Street, Kingston, ON, Canada K7L 3N6

Abstract—Ca^{2+} influx through voltage-gated Ca^{2+} channels is a fundamental signaling event in neurons; however, non-traditional routes, such as non-selective cation channels, also permit Ca^{2+} entry. The present study examines the Ca^{2+} permeability of a cation channel that drives an afterdischarge in *Aplysia* bag cell neurons. The firing of these neurons induces peptide release and reproduction. Single channel-containing inside-out patches excised from cultured bag cell neurons, with the cytoplasmic face bathed in K^+-aspartate and the extracellular face bathed in artificial seawater (11 mM Ca^{2+}), had a reversal potential near +50 mV. In keeping with Ca^{2+} permeability, this was right-shifted to approximately +60 mV in high Ca^{2+} (substituted for Mg^{2+}) and left-shifted to around +40 mV in zero Ca^{2+} (replaced with Mg^{2+}). The current showed inward rectification between +30 and +90 mV, and a conductance of 29 pS in normal Ca^{2+}, 30 pS in high Ca^{2+}, 32 pS in Ba^{2+} (substituted for Ca^{2+}), but only 21 pS in zero Ca^{2+}. Despite a greater conductance in Ba^{2+}, the channel did not display anomalous mol fraction in an equimolar Ca^{2+}–Ba^{2+} mix. Eliminating internal Mg^{2+} lowered activity, but did not alter inward rectification, suggesting intracellular Mg^{2+} is a fast, voltage-independent blocker. Imaging bag cell neurons in Mn^{2+} saline (substituted for Ca^{2+}) revealed enhanced fura-quench following cation channel activation, consistent with Mn^{2+} permeating as a Ca^{2+} surrogate. Finally, triggering the cation channel while tracking capacitance revealed a Ca^{2+}-dependent increase in membrane surface area, consistent with vesicle fusion. Thus, the cation channel not only drives the afterdischarge, but also passes Ca^{2+} to potentially initiate secretion. In general, this may represent an alternate means by which neurons elicit neuropeptide release.

Key words: divalent cation, rectification, capacitance, secretion, reproduction.

*Corresponding author. Tel: +1-613-533-3173; fax: +1-613-533-6880.
E-mail address: magoski@queensu.ca (N. S. Magoski).

Abbreviations: BaASW, Ba^{2+} artificial seawater; CaBaASW, equimolar Ca^{2+}/Ba^{2+} artificial seawater; cfASW, Ca^{2+}-free artificial seawater; cfhmASW, Ca^{2+}-free/high-Mg^{2+} artificial seawater; CtVm, *Conus textile* venom; EGTA, ethyleneglycol bis (aminoethylether) tetraacetic acid; *g*, single-channel conductance; hcmfASW, high Ca^{2+}/Mg^{2+}-free artificial saltwater; Hepes, N-2-hydroxyethlpiperazine-N′-2-ethanesulphonic acid; I_i, initial current; I_{ss}, steady-state current; I–V, current versus voltage; k, slope factor; MnASW, Mn^{2+} artificial sea water; *N*, number of channels in a patch; nASW, normal artificial seawater; NMDA, *N*-methyl-D-aspartate; P_O, single-channel open probability; R_a, access resistance; R_m, membrane resistance; ROI, region of interest; t, time; tcASW, tissue culture artificial seawater; TEA, tetraethylammonium; TFA, trifluoroacetic acid; TRP, transient receptor potential cation channel; t_{tot}, time interval for single-channel open probability measurement; V_{rev}, reversal potential; V_s, voltage step amplitude; $V_{0.5}$, half-maximal voltage of activation; τ, time constant of current decay.

Non-selective cation channels influence membrane potential and firing patterns in sensory, cortical, motor, and peptidergic neurons (Zhang et al., 1995; Haj-Dahmane and Andrade, 1999; Morisset and Nagy, 1999; Hung and Magoski, 2007; Gardam et al., 2008; Tahvildari et al., 2008). As such, these currents impact perception, motor control, memory, and reproduction (Fraser and MacVicar, 1996; Egorov et al., 2002; Hall and Delaney, 2002; Dembrow et al., 2004; Zhang et al., 2008). Cation channels are permeable to Na^+, K^+, and in some cases Ca^{2+} (Yellen, 1982; Partridge and Swandulla, 1988; Strubing et al., 2001; Clapham, 2003). Ca^{2+} permeability broadens their function from simply passing inward current to potentially influencing other processes. For example, while secretion or plasticity are often triggered by voltage-gated Ca^{2+} channels (Mermelstein et al., 2001; Neher and Sakaba, 2008), cation channel–mediated Ca^{2+} entry may initiate secretion from dendrites and synapses, as well as Ca^{2+} release and inflammation in sensory neurons, growth cone turning in spinal neurons, and cell death in cortical or dopaminergic neurons (Chen et al., 1997; Aarts et al., 2003; Munsch et al., 2003; Karai et al., 2004; Yu et al., 2004; Kim et al., 2005; Wang and Poo, 2005; Siemens et al., 2006). The present study examines cation channel Ca^{2+} permeability in the bag cell neurons of the marine snail, *Aplysia californica*.

The bag cell neurons are neuroendocrine cells that control reproduction (Kupfermann, 1967, 1970; Kupfermann and Kandel, 1970). Synaptic input to these neurons activates a non-selective cation channel that drives an ~30 min depolarization and afterdischarge (Kaczmarek et al., 1978; Wilson et al., 1996). This leads to the neurohemal secretion of egg-laying hormone and behaviors ending in egg deposition (Arch, 1972; Pinsker and Dudek, 1977; Rothman et al., 1983; Loechner et al., 1990; Michel and Wayne, 2002). The neurons then become refractory and are incapable of afterdischarging for a prolonged period (Kupfermann and Kandel, 1970; Kaczmarek et al., 1978). Refractoriness likely averts interruption of reproductive behaviors already under way following an initial afterdischarge.

Bag cell neuron depolarization is prevented by either blocking the cation channel or disrupting certain gating factors (DeRiemer et al., 1985; Wilson et al., 1996; Magoski et al., 2002; Kachoei et al., 2006). Cation channel activity is upregulated by elevated intracellular Ca^{2+}, PKC-dependent phosphorylation, or membrane depolarization (Wilson et al., 1996, 1998; Magoski et al., 2002; Magoski, 2004; Magoski and Kaczmarek, 2005; Lupinsky and Magoski, 2006). The channel conducts Na^+ and K^+ to a

0306-4522/09 $ - see front matter
doi:10.1016/j.neuroscience.2009.05.006

similar extent, yet has a current versus voltage (I–V) relationship which extrapolates to a value more positive than 0 mV, suggesting Ca^{2+} permeability (Wilson et al., 1996). In addition, the single-channel current is larger when extracellular Ca^{2+} is replaced by Ba^{2+} (Wilson et al., 1996; Lupinsky and Magoski, 2006), a property often displayed by *bona fide* Ca^{2+} permeable channels (Hagiwara et al., 1974; Hoth, 1995; Hille, 2001). Thus, while the basic function of the cation channel is well established, the extent to which it passes Ca^{2+} and the implications for cellular function are unclear.

Magoski et al. (2000) showed that activating the cation channel in the absence of extracellular Ca^{2+} prevented both refractoriness and the attenuation of intracellular Ca^{2+} release that occurs with repeated stimulation of the bag cell neurons. This too implies that the channel may pass Ca^{2+} and is capable of altering physiology. Using both single-channel recording in excised patches and Ca^{2+} imaging at the whole-cell level, we now show that the cation channel is indeed Ca^{2+} permeable. Furthermore, our data indicate that cation channel–mediated Ca^{2+} influx is capable of initiating secretion in the absence of opening voltage-gated Ca^{2+} channels. Demonstrating that the cation channel passes Ca^{2+} expands its role from driving the afterdischarge to possibly inducing plasticity or peptide release.

EXPERIMENTAL PROCEDURES

Animals and cell culture

Adult *Aplysia californica* weighing 150–500 g were obtained from Marinus Inc. (Long Beach, CA, USA), housed in an ≈300 l aquarium containing continuously circulating, aerated seawater (Instant Ocean, Aquarium Systems, Mentor, OH, USA or Kent sea salt; Kent Marine, Acworth, GA, USA) at 14–16 °C on a 12-h light/dark cycle, and fed romaine lettuce 5 times a week. All experiments were approved by the Queen's University Animal Care Committee (Protocol number Magoski-2005-050-R3). All experiments conformed to the Canadian Council on Animal Care guidelines for the Care and Use of Experimental Animals. Every attempt was made to minimize the number of animals used and their suffering.

For primary cultures of isolated bag cell neurons, animals were anesthetized by an injection of isotonic $MgCl_2$ (50% of body weight), the abdominal ganglion was removed and treated with neutral protease (13.3 mg/ml; 165859; Roche Diagnostics, Indianapolis, IN, USA) for 18 h at 22 °C dissolved in tissue culture artificial seawater (tcASW) (composition in mM: 460 NaCl, 10.4 KCl, 11 $CaCl_2$, 55 $MgCl_2$, 15 Hepes, 1 mg/ml glucose, 100 U/ml penicillin, and 0.1 mg/ml streptomycin, pH 7.8 with NaOH). The ganglion was then transferred to fresh tcASW for 1 h, after which time the bag cell neuron clusters were dissected from their surrounding connective tissue. Using a fire-polished glass Pasteur pipette and gentle trituration, neurons were dispersed in tcASW onto 35×10 mm polystyrene tissue culture dishes (430165; Corning, Corning, NY, USA). Cultures were maintained in tcASW in a 14 °C incubator and used for experimentation within 1–3 days. Salts were obtained from Fisher Scientific (Ottawa, ON, Canada), ICN (Aurora, OH, USA), or Sigma-Aldrich (St. Louis, MO, USA).

Excised, patch-clamp recording

Single cation channel current was measured using an EPC-8 amplifier (HEKA Electronics, Mahone Bay, NS, Canada). Microelectrodes were pulled from 1.5 mm internal diameter, borosilicate glass capillaries (TW 150 F-4; World Precision Instruments, Sarasota, FL, USA) and were fire polished to a resistance of 2–8 MΩ when filled with various salines. To lower the root mean squared noise of the current signal, microelectrode capacitance was reduced by coating the shank and half of the shoulder with dental wax (92189; Heraeus Kulzer, South Bend, IN, USA) under a dissecting microscope.

For inside-out recording, the pipette was filled with normal artificial seawater (nASW) (composition as per tcASW but lacking glucose, penicillin, and streptomycin), high Ca^{2+}/Mg^{2+}-free artificial saltwater (hcmfASW) (Mg^{2+} substituted with Ca^{2+} for a final concentration of 66 mM), Ca^{2+}-free/high-Mg^{2+} artificial seawater (cfhmASW) (Ca^{2+} substituted with Mg^{2+} for a final concentration of 66 mM), CaBaASW (half Ca^{2+} and half Ba^{2+} for a final concentration of 5.5 mM each), or BaASW (Ca^{2+} substituted with Ba^{2+} for a final concentration of 11 mM). In an attempt to reduce contaminating Ca^{2+}-activated K^+ currents, the pipette solution also contained 20 mM tetraethylammonium (TEA) (86630; Sigma-Aldrich). Following excision, the cytoplasmic face was bathed in standard artificial intracellular saline (composition in mM: 500 K-aspartate, 70 KCl, 1.25 $MgCl_2$, 10 Hepes, 11 glucose, 5 EGTA, 10 reduced glutathione, pH 7.3 with KOH). $CaCl_2$ was added for a free Ca^{2+} concentration of 1 μM; calculated using WebMaxC (http://www.stanford.edu/~cpatton/webmaxc/webmaxcE.htm). Experiments performed using zero Mg^{2+} intracellular saline also had a calculated free Ca^{2+} concentration of 1 μM. For outside-out recordings, microelectrodes were filled with standard artificial intracellular saline containing 1 μM free Ca^{2+}. The extracellular face of excised, outside-out patches was exposed to nASW or cfhmASW using a perfusion apparatus (see Experimental procedures, Patch perfusion).

Current was low pass filtered at 1 kHz using the EPC-8 Bessel filter and acquired at a sampling rate of 10 kHz using an IBM-compatible personal computer, a Digidata 1300 analogue-to-digital converter (Axon Instruments/Molecular Devices, Sunnyvale, CA, USA), and the Clampex acquisition program of pCLAMP (version 8.1; Axon Instruments). Data were gathered at room temperature (22 °C) in 0.5–3 min intervals, while holding the patch at various voltages. At more positive potentials, particularly +30 to +90 mV, the time intervals was often ≤1 min because of patch instability and the appearance of large, unidentified, TEA-insensitive outward currents.

Patch perfusion

For patch perfusion, an array was constructed by tightly aligning borosilicate square tubing (outer diameter: 0.75 mm, internal diameter: 0.5 mm; 8250; VitroCom Inc., Mountain Lakes, NJ, USA) attached to one another using superglue. The section of the array that was submerged into the bath did not come in contact with the glue. At the opposite end of the array, the barrels were fitted with silicone tubing (45314; Cole Parmer, Vernon Hills, IL, USA). The perfusion lines were connected to 5 ml syringes, which were all set to the same height. Each line was clamped with an alligator clip, which when released, resulted in a flow of ≈1 ml/min. Patches were moved from the mouth of one barrel to the next, permitting a rapid change in solutions at the channel face. During perfusion, the culture dish was drained as required using a plastic Pasteur pipette. Prior to experimentation, the entire perfusion system was rinsed with Sigmacote (SL-2; Sigma-Aldrich) and allowed to dry for at least 24 h.

Conus textile venom (CtVm)

To activate the cation channel macroscopically, crude CtVm (Cruz et al., 1976) was bath applied to cultured bag cell neurons (Wilson et al., 1996; Magoski et al., 2000, 2002). CtVm lyophilate was generously provided by Ms. J. Imperial and Dr. B. M. Olivera of the University of Utah. Adult specimens of the molluscivorous snail, *Conus textile*, were collected from the ocean around the Philippine

island of Marinduque. Venom ducts were dissected out of an animal and placed on an ice cold metal spatula. The duct was then cut into 2 cm sections and the venom extruded out by squeezing with forceps. CtVm was then lyophilized in a vacuum centrifuge and stored at −80 °C for subsequent extraction. Crude CtVm was extracted at 4 °C by adding 0.5% v/v trifluoroacetic acid (TFA) (T6508; Sigma-Aldrich) to the lyophilate for a final protein concentration of 5% (w/v). CtVm was vortexed for 2 min and sonicated for 2 min, in an alternating fashion, for a total of 18 min. The mixture was then centrifuged at 15,000×*g* for 12 min and the supernatant collected. A second aliquot of TFA was added to the pellet (final protein concentration 10% w/v) and the protocol repeated. The supernatants were pooled, aliquoted and frozen at −80 °C. CtVm was introduced into the bath by pipetting a small volume (<10 μl) of the stock into the culture dish for a final protein concentration of ≈100 μg/ml. Care was taken to pipette the stock near the side of the dish and as far away as possible from the neuron.

Whole-cell voltage-clamp and Mn^{2+}-fura quench

Fura PE3 dye (K^+ salt; 0110, Teflabs, Austin, TX, USA) (Vorndran et al., 1995), was pressure injected via sharp-electrode (1.2 mm internal diameter, borosilicate glass capillaries, 1B120F-4; World Precision Instruments; 30–50 MΩ resistance when tip-filled with 10 mM fura-PE3 and backfilled with 3 M KCl) using a PMI-100 pressure microinjector (Dagan, Minneapolis, MN, USA), while simultaneously monitoring membrane potential with an Axoclamp 2 B amplifier (Axon Instruments). To dye-fill a neuron usually required 10–15, 300–900 ms pulses at 30–60 kPa to, which were subsequently allowed to equilibrate for at least 30 min prior to experimentation. Dye-filled neurons were subsequently whole-cell voltage-clamped at −60 mV using the Axoclamp and the continuous voltage-clamp mode. Current was low pass filtered at 3 kHz using the Axoclamp Bessel filter and acquired at a sampling rate of 2 kHz. Whole-cell microelectrodes (glass as per single-channel recording) were fire polished to a resistance of 1.5–3 MΩ when filled with standard artificial intracellular saline (composition as per single-channel recording but with 1 mM fura-PE3, 5 mM ATP (grade 2, disodium salt; A3377; Sigma-Aldrich), 100 μM guanosine triphosphate (GTP) (type 3, disodium salt; G8877; Sigma-Aldrich), and free Ca^{2+} set to 300 nM). We found that pre-loading the neurons by fura microinjection as well as including fura in the whole-cell pipette resulted in stable dye concentrations during recording.

Imaging was performed simultaneously with voltage-clamp, using a Nikon TS100-F inverted microscope (Nikon, Mississauga, ON, Canada) equipped with a Nikon Plan Fluor 40X (NA=0.6) objective. The light source was a 75 W xenon arc lamp and a multi-wavelength DeltaRAM V monochromatic illuminator (Photon Technology International, London, ON, Canada) coupled to the microscope with a UV-grade liquid-light guide. The excitation wavelength was 358 nm and was controlled by an IBM-compatible personal computer, a Photon Technology International computer interface, and ImageMaster Pro software (version 1.49, Photon Technology International). Between acquisition episodes, the excitation wavelength was blocked by a computer-controlled shutter. The emitted light passed through a 510/40 nm barrier filter prior to being detected by a Photon Technology International IC200 intensified charge-coupled device camera. The camera intensifier voltage was set based on the initial fluorescence intensity of the cells at the beginning of each experiment and maintained constant thereafter. The camera black level was set prior to an experiment using the camera controller such that at a gain of 1 and with no light going to the camera there was a 50:50 distribution of blue and black pixels on the image display. Fluorescence intensities were sampled at 20 s intervals using regions of interests (ROI) defined over the neuronal somata prior to the start of the experiment and averaged four to eight frames per acquisition. The emission was recorded as an indicator of fura PE3 quench by Mn^{2+}. The black level determination, image acquisition, frame averaging, and ROI sampling were carried out using the ImageMaster Pro software. Imaging was undertaken at ≈22 °C and performed in Mn^{2+} artificial sea water (MnASW) with the $CaCl_2$ replaced by $MnCl_2$ for a final concentration of 11 mM. Mn^{2+} acts as a surrogate for Ca^{2+}, whereby any Mn^{2+} entry through Ca^{2+} permeable channels is detected by quenching of the fura. Mn^{2+}, but not Ca^{2+}, quenches fura when monitored at its isosbestic point (358 nm; Grynkiewicz et al., 1985), and thus differentiates between Ca^{2+} release and Ca^{2+} influx (Hallam and Rink, 1985; Sage et al., 1989).

Capacitance tracking

As an indicator of secretion, membrane capacitance was tracked under whole-cell voltage-clamp using the time-domain method (Neher and Marty, 1982; Gillis, 1995). Whole-cell recording conditions were the same as during imaging except the internal lacked fura-PE3 and the EPC-8 amplifier was used. The holding potential was −80 mV, from which +20 mV, 100 ms pulses were delivered at 0.5 Hz. With pipette capacitance compensated, the membrane test function of Clampfit was employed to calculate membrane capacitance on-line using the formula: membrane capacitance (C_m)=$\tau(1/R_a+1/R_m)$, where τ=time constant of current decay as fit by a single-exponential from initial to steady-state during the voltage step, R_a=access resistance, and R_m=membrane resistance. R_a was calculated using the formula: $R_a=V_s/I_i$, where V_s=voltage step amplitude (20 mV) and I_i=the initial current flowing during the step. R_m was calculated using the formula: $R_m=(V_s-R_a\times I_{ss})/I_{ss}$, where I_{ss}=the steady-state current flowing during the step. To increase accuracy and improve the signal-to-noise ratio, current traces were cumulatively averaged (10 pulses per average) before each calculation. The −80 mV holding potential was chosen to avoid activation of any voltage-gated Ca^{2+} channels during the 20 mV step (Tam and Magoski, 2007). Data were gathered at ≈22 °C.

Analysis

To determine single-channel open probability (P_O), events lists were made from data files using the half-amplitude threshold criterion (Colquhoun and Sigworth, 1995) and the Fetchan analysis program of pCLAMP. Fetchan was also used to generate all-points histograms for determining channel amplitude. For analysis, most data did not require further filtering below the 1 kHz used during acquisition; however, to avoid inclusion of noise-related "events" as channel openings, some data were filtered a second time using the Fetchan digital gaussian filter to a final cutoff frequency of 500–200 Hz. The lower frequency filtering was typically carried out on small amplitude currents acquired at voltages near the reversal potential. For display in figures most data were filtered to a final cutoff frequency of 500 or 250 Hz. The Pstat analysis program of pCLAMP was used to read events lists and determine P_O using the formula: $P_O=(1\times t_1+2\times t_2+\ldots t_n)/(N\times t_{tot})$, where t=the amount of time that n. channels are open, N=the number of channels in the patch, and t_{tot}=the time interval over which single-channel open probability is measured. Channel number was determined by counting the number of unitary current levels at the most positive voltage of a given recording. Pstat was also used to fit gaussian functions to all-points histograms using the least squares method and a simplex search. Channel current amplitude was then calculated by subtracting the mean closed current level from the mean open current level at a given voltage.

Single-channel I–V relationships were produced in Origin (version 7; OriginLab Corporation, Northampton, MA, USA) by plotting channel current amplitude against patch holding potential. Single-channel conductance (g) and reversal potential (V_{rev}) were determined by linear regression. To make P_O versus voltage relationships, P_O was first normalized to P_O at 0 mV and then plotted against patch holding potential using Origin. This relation-

ship was then fit with a Boltzmann function to derive the half-maximal voltage of activation ($V_{0.5}$) and the slope factor (k), which is the change in voltage required to move the P_O *e*-fold. We chose to normalize to P_O at 0 mV, rather than the more positive potentials, because this voltage has been used in the past as the point of reference (Wilson et al., 1996; Magoski, 2004; Lupinsky and Magoski, 2006). Moreover, the short recording times necessary when holding between +30 and +90 mV (see Experimental Procedures, Excised patch-clamp recording) reduced the certainty of the P_O calculations for those voltages. As such, we felt it not prudent to normalize to P_O measured above 0 mV.

Whole-cell cation channel activation and simultaneous Mn^{2+} influx were quantitated with the Clampfit analysis program of pCLAMP and Origin, respectively. For current, cursors were placed at the baseline, prior to CtVm introduction, as well as at the peak after the cation channel had been activated. The difference between the two cursor values was taken as the maximal amplitude. For Mn^{2+} influx, fura quench emission records from ImageMaster Pro were plotted in Origin and fit with single exponential to derive time constant values that reflected the rate of fura quench by Mn^{2+} entry.

Data are presented as mean±standard error of the mean (SEM) throughout. Statistical analysis was performed using InStat (version 3; GraphPad Software, San Diego, CA, USA). The Kolmogorov–Smirnov method was used to test data sets for normality. Paired Student's *t*-test or Mann–Whitney *U*-test was used to test whether the mean differed between two groups. A one-sample *t*-test was used to determine if a single mean differed from that of zero. Means were considered significantly different if the two-tailed *P*-value was <0.05.

RESULTS

Altering extracellular Ca^{2+} shifts cation channel reversal potential and conductance

In their initial characterization of the bag cell neuron cation channel, Wilson et al. (1996) demonstrated a roughly equal permeability to Na^+ and K^+; moreover, when they replaced extracellular Na^+ with large, impermeable monovalent cations, the V_{rev} was shifted in a positive direction, suggesting Ca^{2+} permeability. However, those authors did not examine the current at holding potentials more positive than 0 mV, but instead extrapolated the linear regression to estimate V_{rev}. Here, we used excised patches to test if the cation channel passes Ca^{2+} under more physiological ionic conditions (high Na^+ outside and high K^+ inside) by holding both below and well above 0 mV to determine V_{rev}.

Cation channels were identified in excised, inside-out patches from cultured bag cell neurons based on properties previously reported by both our laboratory and others, i.e. ≈2 pA current amplitude at −60 mV, voltage-dependent activation (an increase in P_O with depolarization), and lack of voltage-dependent inactivation (Wilson and Kaczmarek, 1993; Wilson et al., 1996, 1998; Magoski et al., 2002; Magoski, 2004; Lupinsky and Magoski, 2006). With nASW (11 mM Ca^{2+} and 55 mM Mg^{2+}) at the extracellular face and standard intracellular saline at the cytoplasmic face, the cation channel showed inward current from −90 through to +30 mV (Fig. 1A). A further change in holding potential to +60 mV saw the current go to zero and then reverse by +90 mV. The I–V curve displayed inward rectification at voltages positive to −30 mV, which manifested as a modest but conspicuous decrease in slope (Fig. 1B). When the P_O was normalized to the P_O at 0 mV and the single-channel activation curve fit with a Boltzmann function, the $V_{0.5}$ was −40 mV and the k was 8 (Fig. 1C).

If the cation channel was indeed permeable to Ca^{2+}, then the single-channel *g* and V_{rev} should be sensitive to changes in extracellular face Ca^{2+} concentration. We substituted Ca^{2+} for Mg^{2+} and vice versa in the ASW used to fill the pipettes for excised inside-out patches. The current amplitude of the channel was attenuated with cfhmASW (0 mM Ca^{2+}, 66 mM Mg^{2+}) and enhanced with hcmfASW (66 mM Ca^{2+}, 0 mM Mg^{2+}) at the extracellular face (Fig. 2A). As with nASW, inward rectification of the I–V curve was observed at positive voltages in both cfhmASW and hcmfASW. Therefore, the data were separated and linear regression was carried out on I–V relationships from either −90 to −30 mV (the slope providing the *g* in the physiological operating range of the channel) or 0 to +90 mV (the X-intercept providing the V_{rev}). Cation channel *g* was attenuated and enhanced by low and high external Ca^{2+}, respectively. The *g* derived from the I–V at negative voltages was 29.2 pS in nASW, which was reduced to 21.4 pS in cfhmASW and increased somewhat to 30.3 pS in hcmfASW (Fig. 2B). The V_{rev} obtained from the I–V at positive voltages was similarly sensitive to changes in extracellular Ca^{2+}, shifting from +53.0 mV in nASW to +41.1 mV in cfhmASW or +59.3 mV in hcmfASW (Fig. 2C).

Cation channel conductance is enhanced by extracellular Ba^{2+}, but fails to display anomalous mol fraction

Many Ca^{2+} permeable channels also conduct Ba^{2+}, often more effectively than Ca^{2+} itself (Hagiwara et al., 1974; Hoth, 1995; Hille, 2001). Both Wilson et al. (1996) and our laboratory (Lupinsky and Magoski, 2006) showed that the amplitude of the bag cell neuron cation channel was increased by replacing extracellular Ca^{2+} with Ba^{2+} at −60 mV. Indeed, this was the only prior evidence to suggest the cation channel is Ca^{2+} permeable under physiological ionic conditions. It has been proposed that Ca^{2+} permeable channels are multi-ion pores, i.e. they can hold more than one divalent ion simultaneously (Hess and Tsien, 1984; Hille, 2001). To explore this, we first determined single-channel *g* with BaASW (0 mM Ca^{2+}, 11 mM Ba^{2+}) at the extracellular face in excised, inside-out patches. As expected, having Ba^{2+} as the only permeable divalent cation on the outside of the channel brought about a larger current amplitude between −90 and −30 mV. However, when the equimolar mixture of CaBaASW (5.5 mM Ca^{2+}, 5.5 mM Ba^{2+}) was presented to the extracellular face, the current was essentially the same magnitude as that seen with nASW (Fig. 3A–C; compare to Fig. 1A).

The linear regression of the I–V at negative voltages showed *g* to be larger (31.8 pS) with BaASW (Fig. 3D). However, with a *g* of 29.6 pS in CaBaASW versus 29.2 pS in nASW, the channel did not exhibit the anomalous mol fraction effect of a smaller conductance in an equimolar Ca^{2+}–Ba^{2+} mix (Hess and Tsien, 1984; Friel and Tsien, 1989; Hille, 2001). With respect to V_{rev}, compared to +53.0 mV in nASW, the linear regression of the I–V at

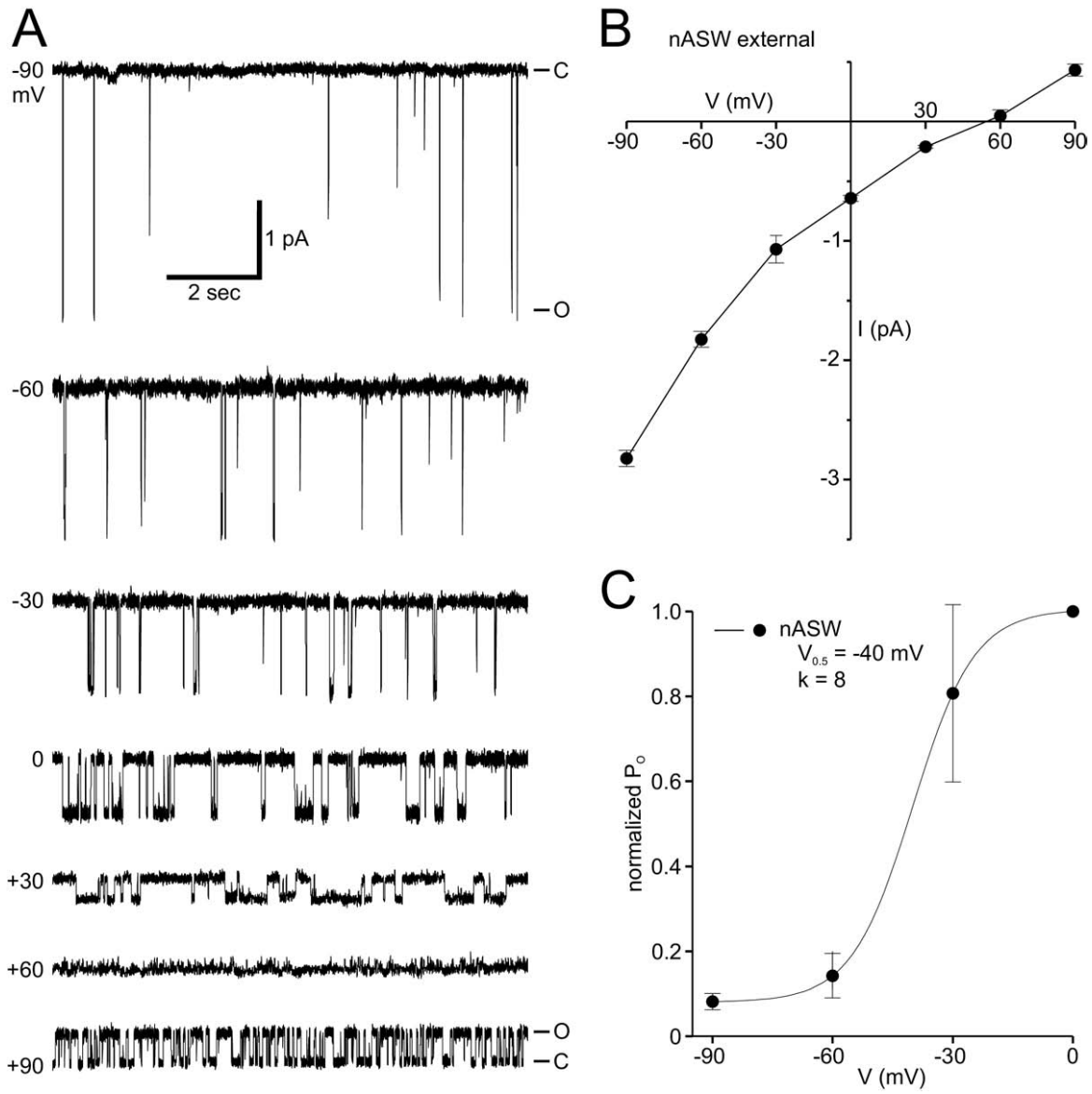

Fig. 1. Cation channel activity and I–V relationship in control conditions. (A) Single cation channel in an excised, inside-out patch at different holding potentials with nASW (11 mM Ca^{2+} and 55 mM Mg^{2+}) at the extracellular face. The cation channel is seen as brief, unitary, inward current deflections of close to 3 pA at −90 mV. The closed and open states are designated by −C and −O, respectively. From −90 mV through to +30 mV, the amplitude of the inward current decreases, while the number of openings increases. There are no resolvable openings at +60 mV, but at +90 mV the current reverses and shows outward openings. For all holding potentials, the current exhibits no voltage-dependent inactivation. (B) The I–V of the single-channel current rectifies at voltages more positive than −30 mV, with a distinct reduction in slope. Channel current amplitude at each voltage is obtained from gaussian fits of all-points histograms (see Experimental Procedures, Analysis). The number of patches at holding potentials of −90, −60, −30, 0, +30, +60, and +90 mV, is n=6, 5, 6, 6, 6, 4, and 4, respectively. (C) Single-channel activation curve with P_O normalized to P_O at 0 mV and fit with a Boltzmann function. P_O is determined for the total time at the given holding potentials (see Experimental Procedures, Analysis). Number of patches is n=6, 5, 6, 6 for −90, −60, −30, and 0 mV, respectively.

positive voltages provided a value of +46.6 mV in BaASW and +48.0 mV in CaBaASW (data not shown). The single-channel activation curves in either CaBaASW or BaASW were noticeably shifted to the right (Fig. 3E). Estimates of $V_{0.5}$ from the Boltzmann fits +59.0 mV in CaBaASW and +69.0 mV in BaASW, with k-values of 25 and 26, respectively. These shifts were quite drastic and the fit to the CaBaASW or BaASW curves should be interpreted judiciously.

Intracellular Mg^{2+} regulates cation channel activity but is not responsible for inward rectification

The inward rectification seen in the bag cell neuron cation channel I–V at positive voltages is reminiscent of other channels, including exogenously expressed transient receptor potential (TRP) cation channel isoforms (Voets et al., 2003; Hermosura et al., 2005; Obukhov and Nowycky, 2005) and native cation channels (Inoue et al., 2001;

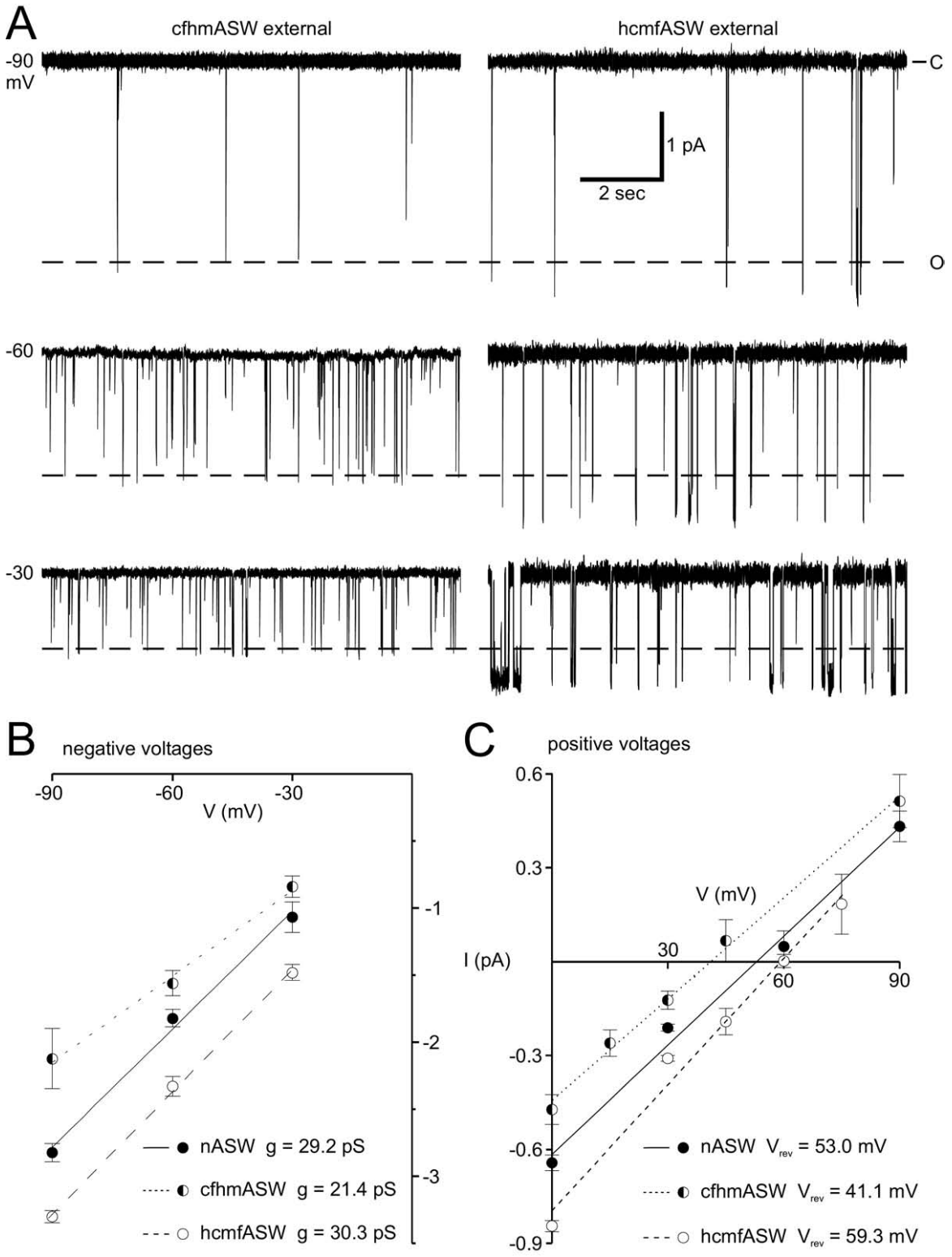

Fig. 2. The conductance and reversal potential of the cation channel is sensitive to changes in extracellular Ca^{2+}. (A) Sample traces at holding potentials of −90, −60, and −30 mV of single cation channels in excised, inside-out patches with either cfhmASW (0 mM Ca^{2+}, 66 mM Mg^{2+}) or hcmfASW (66 mM Ca^{2+}, 0 mM Mg^{2+}) at the extracellular face. The dashed lines designate the open state for the channel in cfhmASW. These lines intersect with the current traces in hcmfASW at all voltages, demonstrating the amplitude is larger with high Ca^{2+}. The scale bar applies to both panels. (B) The I–V at negative voltages in both Ca^{2+}-free (half-closed circles, small-dashed line) and high-Ca^{2+} (open circles, large-dashed line) conditions, as well as normal Ca^{2+} (closed circles, solid line; re-plotted from Fig. 1). Each relationship is fit with a linear regression to determine single-channel *g*.

Strong and Scott, 1992). In some of these cases, this phenomenon is due a voltage-dependent block by intracellular Mg^{2+}. We examined this possibility in excised inside-out, cation-channel-containing patches with nASW at the extracellular face and zero Mg^{2+} intracellular saline (no added Mg^{2+}) at the cytoplasmic face. When compared to the single channel I–V recorded using standard intracellular saline (1.25 mM Mg^{2+}; see Fig. 1B) there was no change in the shape of the curve, i.e. the inward rectification at positive voltages was still apparent (Fig. 4A). Not surprisingly, the V_{rev} was +54.9 mV when intracellular Mg^{2+} was removed (linear regression not shown), a value similar to +53.0 mV with normal Mg^{2+}. However, an absence of Mg^{2+} at the cytoplasmic face was not entirely without effect. In additional experiments, inside-out patches were held at −60 mV and perfused with regular versus zero Mg^{2+} intracellular saline. In these cases, cation channel P_O was enhanced in the absence of Mg^{2+} (Fig. 4B, C).

Cation channel activation at the whole-cell level produces Ca^{2+} entry

Our single-channel data indicated that the bag cell neuron cation channel is Ca^{2+} permeable under physiological ionic conditions. To look at this at the whole-cell level, we activated the cation channel with venom from the marine snail, *Conus textile*, while imaging Ca^{2+} influx with fura quench. CtVm activates the cation channel through a membrane receptor and intracellular pathway (Wilson and Kaczmarek, 1993; Magoski et al., 2002; Kachoei et al., 2004, 2006). However, CtVm also releases Ca^{2+} from intracellular stores (Magoski et al., 2000); thus, it was important to distinguish between Ca^{2+} influx and Ca^{2+} release. To do so, fura-PE3-loaded cultured bag cell neurons were imaged at 358 nm while voltage-clamped at −60 mV. This wavelength is the isosbestic point of fura, where fluorescence intensity is not sensitive to Ca^{2+} but determined only by the dye concentration (Grynkiewicz et al., 1985). Replacing extracellular Ca^{2+} with Mn^{2+} allows it to act as a surrogate and flow through any Ca^{2+} permeable channels. When fura binds Mn^{2+} it quenches the dye and effectively reduces its concentration (Hallam and Rink, 1985; Sage et al., 1989). Hence, even if CtVm liberates intracellular Ca^{2+}, only Ca^{2+} (i.e. Mn^{2+}) entry will be detected. Moreover, holding at −60 mV prevents the CtVm-activated cation channel from depolarizing the neuron and confounding the assay by opening voltage-gated Ca^{2+} channels.

We examined the Mn^{2+} permeability of the cation channel by making inside-out recordings with MnASW (0 mM Ca^{2+}, 11 mM Mn^{2+}) as the external saline. The cation channel I–V with MnASW was very similar to that observed with nASW (Fig. 5A). Moreover, linear regression (not shown) of the MnASW I–V provided a *g* of 29.3 pS at negative voltages, which is essentially the same as 29.2 pS seen with nASW, and a V_{rev} of +48.2 mV at positive voltages, which is somewhat smaller than the control value of +53.0 mV. This suggests that the cation is permeable to Mn^{2+}, although slightly less than that for Ca^{2+}. If Mn^{2+} did not pass through the channel, then the conductance and reversal potential would have behaved as if Ca^{2+} were absent and shifted to values similar to that seen with cfhmASW.

To test that Mn^{2+} influx could indeed quench fura fluorescence in bag cell neurons, a positive control was performed by depolarizing the membrane potential for a prolonged period to intentionally activate voltage-gated Ca^{2+} channels. In MnASW, a 10 s step depolarization from −60 mV to +10 mV under voltage-clamp induced pronounced Mn^{2+} influx as measured by the rapid quench of fura-PE3 (Fig. 5B). In other neurons, CtVm (100 μg/ml) was applied under continuous voltage-clamp at −60 mV. When compared to water, the vehicle, this produced a conspicuous inward current consistent with activation of the cation channel as reported by others (Wilson et al., 1996; Magoski et al., 2000) (Fig. 5C). Moreover, CtVm application resulted in prominent Mn^{2+} influx as demonstrated by a significantly shorter time constant of fura quench (Fig. 5D).

Removal of extracellular Ca^{2+} lowers cation channel activity

What are the roles of cation channel–mediated Ca^{2+} entry in bag cell neurons? One possibility comes from our prior work showing that extracellular Ba^{2+} decreased P_O (Lupinsky and Magoski, 2006). In addition to voltage, the cation channel is gated by Ca^{2+} through a close association with calmodulin. We concluded that Ca^{2+} normally flowing through the channel also serves as a gating factor, and this stimulation was not recapitulated by Ba^{2+} because it activates calmodulin poorly (Haiech et al., 1981; Chao et al., 1984; Wang, 1985; Ozawa et al., 1999). This is reminiscent of the effect of Ba^{2+} on Ca^{2+}-dependent inactivation of voltage-gated Ca^{2+} channels (Tillotson, 1979; Eckert and Tillotson, 1981; Zuhlke et al., 1999). However, as shown in the present study, Ba^{2+} also right-shifted bag cell neuron cation channel voltage-dependence (see Fig. 3D), and the effect on P_O may not necessarily have been due to a lack of Ca^{2+} influx.

To better resolve if Ca^{2+} influx provides positive feedback to the bag cell neuron cation channel, excised, outside-out patches were made with standard intracellular saline in the pipette, held at −60 mV, and the extracellular face perfused with nASW (11 mM Ca^{2+} and 55 mM Mg^{2+}) followed by cfhmASW (0 mM Ca^{2+}, 66 mM Mg^{2+}). Fig. 6A shows how removal of extracellular Ca^{2+} decreased cat-

Compared to control, *g* is clearly smaller without extracellular Ca^{2+}, and slightly larger in high Ca^{2+}. (C) The I–V at positive voltages in both Ca^{2+}-free (half-closed circles, small-dashed line) and high-Ca^{2+} (open circles, large-dashed line), as well as normal Ca^{2+} (closed circles, solid line; re-plotted from Fig. 1). The linear regression fits to these relationships yield a V_{rev} that, in contrast to normal Ca^{2+}, is right-shifted in high Ca^{2+} and left-shifted in zero Ca^{2+}. The number of patches for cfhmASW is 10, 12, 12, 12, 10, 6, 6, 6 for −90, −60, −30, 0, +15, +30, +45, and +90 mV, respectively, while for hcmfASW it is 9, 10, 9, 8, 7, 2, 4, 3 for −90, −60, −30, 0, +30, +45, +60, and +75 mV, respectively.

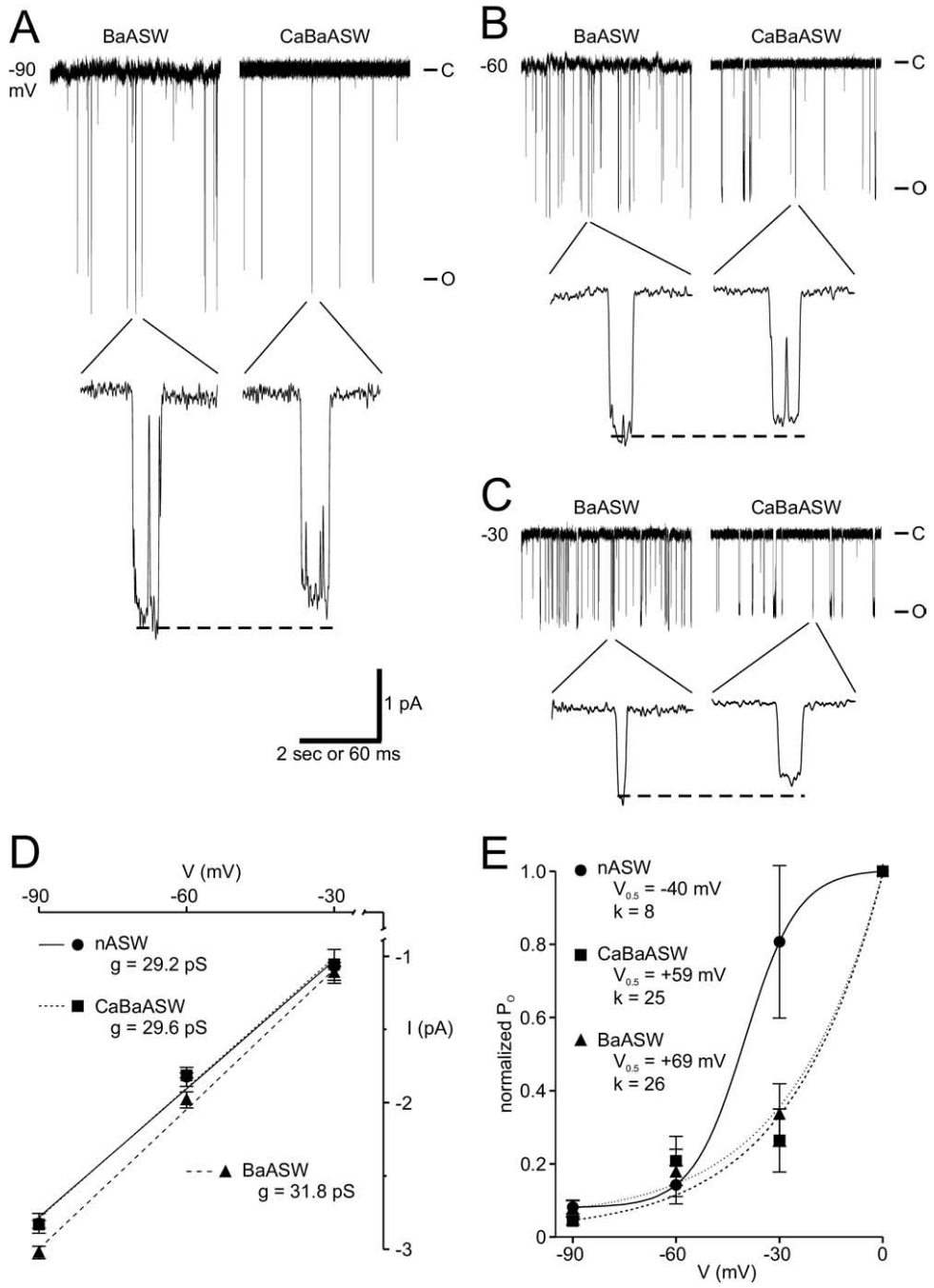

Fig. 3. Substitution of extracellular Ca^{2+} with Ba^{2+} increases cation channel conductance and right-shifts voltage-dependence. (A–C) Representative traces at holding potentials of −90, −60, and −30 mV of single cation channels in excised, inside-out patches with either BaASW (*left*, 0 mM Ca^{2+}, 11 mM Ba^{2+}) or CaBaASW (*right*, 5.5 mM Ca^{2+}, 5.5 mM Ba^{2+}) at the extracellular face. The scale bars apply to A–C. *Upper panels*, 10 s samples of cation channel activity. The current amplitude is greater if Ca^{2+} is fully replaced by Ba^{2+}. The 2 s time base applies. *Lower panels*, 100 ms samples of cation channel activity taken from the upper panels as indicated. The dashed lines designate the open state for the channel in BaASW. These lines fail to intersect the current traces in CaBaASW at any voltage, establishing that the amplitude is smaller in the mixed divalent saline. The 60 ms time base applies. (D) The I–V at negative voltages in Ba^{2+} only (triangles, small-dashed line), an equal Ca^{2+}–Ba^{2+} mix (squares, dotted line), and normal Ca^{2+} (circles, solid line; re-plotted from Fig. 1). Compared to control, the *g* is distinctly larger in full extracellular Ba^{2+}, but largely unchanged in the Ca^{2+}–Ba^{2+} mix. (E) Single-channel activation curves (P_O normalized to P_O at 0 mV) in normal Ca^{2+} (re-plotted from Fig. 1), a Ca^{2+}–Ba^{2+} mix, and full extracellular Ba^{2+}. Fitting the curves with a Boltzmann function fit provides $V_{0.5}$ values that are markedly right-shifted in either CaBaASW or BaASW. Similarly, the k under both of these conditions is far less steep than control. Given the extent of the shift with either CaBaASW or BaASW, the $V_{0.5}$ and k-values should be interpreted as estimates. Number of patches in CaBaASW is n=5, 5, 5, 5 and BaASW is n=6, 7, 6, 7 for −90, −60, −30, and 0 mV, respectively.

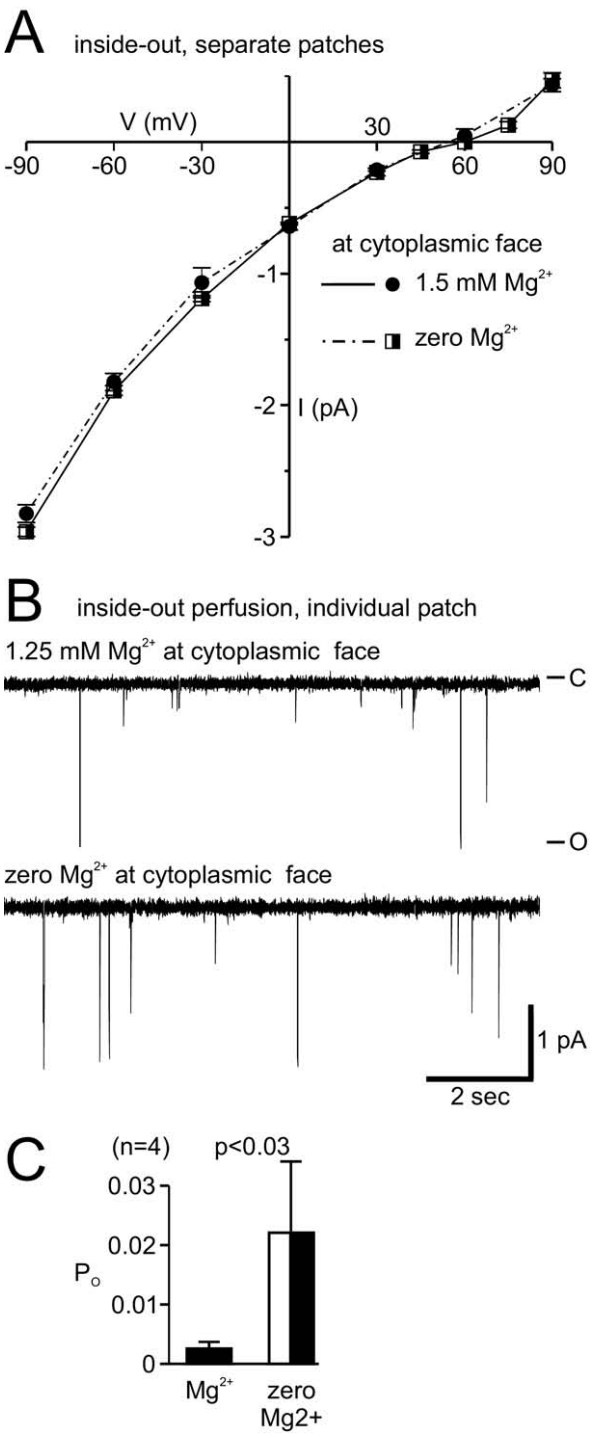

Fig. 4. Removal of cytoplasmic face Mg^{2+} lowers cation channel activity but does not alter conductance or reversal potential. (A) Single cation channel I–V in excised, inside-out patches with zero Mg^{2+} intracellular saline (half-closed squares, dashed dotted line) or standard (1.5 mM Mg^{2+}) intracellular saline (circles, solid line; re-plotted from Fig. 1) at the intracellular face. The extracellular face is exposed to nASW in both sets of experiments. Neither the shape of the relationship, nor the V_{rev} is altered to any great extent. For the Mg^{2+}-free intracellular saline number of patches at holding potentials of −90, −60, −30, 0, +30, +45, +60, +75, and +90 mV, is n=6, 6, 6, 6, 6, 4, 5, 4, and 5, respectively. (B) In a separate set of experiments, inside-out patches are voltage-clamped at −60 mV and perfused with regular and then zero Mg^{2+} intracellular saline. Removal of Mg^{2+} from the cytoplasmic face elevates cation channel activity. (C) Summary data show that mean cation channel P_O increases with zero Mg^{2+} intracellular saline to a level that reaches significance when compared to control (Mann–Whitney U-test).

ion channel P_O, which amounted to an average two-thirds reduction that readily met the level of significance.

We are confident that the channels observed in outside-out patches are the same as those seen in the inside-out configuration because they have the same ≈2 pA current amplitude at −60 mV and present the same mean open time (5.8±1.1 vs. 11.9±5.2 ms; not significant, Mann–Whitney U-test; n=4 and 4). Wilson et al. (1996) managed to obtain a cation channel g of 29.1 pS using outside-out patches, which is very close to the 29.2 pS g we found with inside-out patches. Finally, we previously reported currents in outside-out patches that were similar in amplitude and kinetics to that described in the present study; moreover, as is the case for inside-out channels, those currents were Ca^{2+}-sensitive, with P_O varying as a function of cytoplasmic face Ca^{2+} concentration (Lupinsky and Magoski, 2006).

To be certain that replacing Ca^{2+} with Mg^{2+} did not simply alter voltage-dependence, we analyzed data from excised, inside-out patches with nASW or cfhmASW at the extracellular face (see also Figs. 1 and 2). Not surprisingly, a plot of straight P_O versus voltage revealed that, in separate patches, cation channels in nASW had larger average activity at all voltages compared to those in cfhmASW (Fig. 6B). However, when P_O was normalized to P_O at 0 mV, the single-channel activation curve in cfhmASW was very similar to that of nASW (Fig. 6C). A Boltzmann fit to the cfhmASW curve yielded a $V_{0.5}$ of −37 mV and a k of 9, which were not appreciably different from what was originally observed in nASW.

Cation channel activation initiates a Ca^{2+}-dependent increase in membrane capacitance

In addition to potentially regulating the channel itself, Ca^{2+} influx through the cation channel may give rise to other intracellular processes. We tested the hypothesis that cation channel–mediated Ca^{2+} influx can also initiate secretion. Work by both our laboratory (Hickey et al., 2008) and others (Jo et al., 2007) indicates that stimulation of cultured bag cell neurons with elevated extracellular K^+ or strong depolarization under voltage clamp results in Ca^{2+} entry through voltage-gated Ca^{2+} channels and peptide release. For the present study, neurons were held at −80 mV and membrane capacitance was tracked as an index of secretion (Neher and Marty, 1982; Lim et al., 1990; Gillis, 1995).

As was done for the Mn^{2+} quench/Ca^{2+} influx experiments, the cation channel was triggered by application of CtVm. In keeping with cation channel–mediated Ca^{2+} entry initiating peptide release, Fig. 7A shows channel activation in nASW (11 mM Ca^{2+}) produced a slow increase in capacitance (n=14). However, with Ca^{2+}-free artificial seawater (cfASW) (0 mM Ca^{2+}) as the extracellular me-

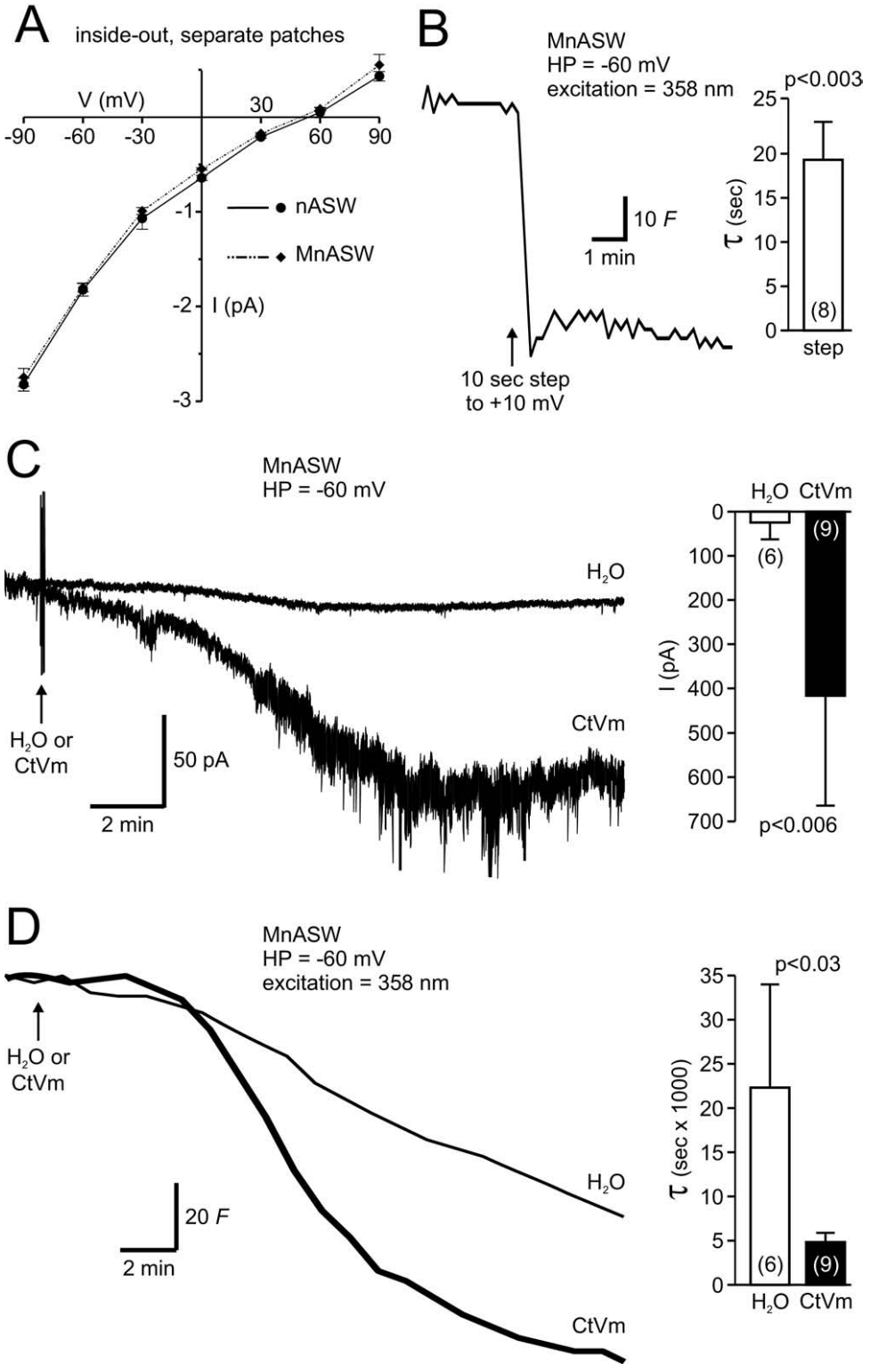

Fig. 5. Bag cell neuron Mn^{2+} influx is enhanced by cation channel activation. (A) Single cation channel I–V in excised, inside-out patches with MnASW (0 mM Ca^{2+}, 11 mM Mn^{2+}; diamonds, dashed double-dotted line) or nASW (11 mM Ca^{2+}; circles, solid line; re-plotted from Fig. 1) at the extracellular face. Neither the shape of the relationship, nor the V_{rev} is appreciably changed by the presence of Mn^{2+}. For MnASW, the number of patches at holding potentials of −90, −60, −30, 0, +30, +60, and +90 mV, is n=6, 8, 7, 4, 4, 7, and 5, respectively. (B) Fura PE3-loaded neurons are voltage-clamped at a holding potential (HP) of −60 mV in MnASW. At the isosbestic point (358 nm), intensity is directly related to dye concentration, and quenching of fura by Mn^{2+}, but not Ca^{2+}, differentiates between Ca^{2+}-release and Mn^{2+} influx. *Left*, Rapid quenching occurs following brief depolarization to +10 mV (at arrow) and Mn^{2+} influx through voltage-gated Ca^{2+} channels. *Right*, Summary data of voltage-gated Mn^{2+} influx, which is significantly different

dium, CtVm caused either no change or only a very gradual reduction in capacitance ($n=6$). Interestingly, in the majority of neurons recorded with nASW ($n=10$ of 14) there was a relatively rapid, transient decrease in capacitance prior to the inevitable increase. This temporary lowering of capacitance was never observed in the neurons recorded in cfASW. The average peak change in capacitance with nASW was significantly different when compared to that with cfASW (Fig. 7B).

DISCUSSION

The activation of cation channels by Ca^{2+}, depolarization, and/or receptor pathways impacts membrane potential, excitability, and spike rate in neurons from many species (Kramer and Zucker, 1985; Partridge et al., 1994; Congar et al., 1997; Haj-Dahmane and Andrade, 1999; Morisset and Nagy, 1999; Raman et al., 2000; Perrier and Hounsgaard, 2003; Clapham, 2003; Magoski and Kaczmarek, 2004; Lu et al., 2009; Putzier et al., 2009). In the bag cell neurons, a cation channel provides much of the inward current for an afterdischarge that elicits egg-laying (Kaczmarek and Strumwasser, 1984; Wilson et al., 1996). At both the whole-cell and single-channel level this current is non-selective for monovalent cations, Ca^{2+}- and voltage-activated, as well as non-inactivating (Wilson et al., 1996; Magoski, 2004; Lupinsky and Magoski, 2006). We now demonstrate that the cation channel is Ca^{2+} permeable and provide evidence consistent with this Ca^{2+} influx both regulating the channel itself and causing secretion.

Our control recordings of the cation channel in excised-inside-out patches reveal a rather positive V_{rev} of $+53$ mV. Moreover, the elevated Ca^{2+} of hcmfASW right-shifts V_{rev} and increases single-channel g, whereas these measures are left-shifted and decreased, respectively, by the low Ca^{2+} of cfhmASW. Given that the Ca^{2+} Nernst potential in our control conditions is $\approx+115$ mV, these results are consistent with a current that, while permeable to Na^+ and K^+, also passes Ca^{2+}. The contribution of Ca^{2+} to the current is not small, as low Ca^{2+} reduces g by over 25%. Clearly, the extent of Ca^{2+} permeability will affect the amount of inward current and strength of excitation.

Ba^{2+} permeability is a common property of channels that carry Ca^{2+} (Hagiwara et al., 1974; Hoth, 1995; Hille, 2001). The bag cell neuron cation channel is no exception, with a higher single-channel g and more negative V_{rev} in BaASW compared to nASW. Hess et al. (1986) proposed that Ba^{2+} currents are larger and display a left-shifted V_{rev} because Ba^{2+} has a lower affinity than Ca^{2+} for specific binding site(s) in the pore. Lower affinity confers larger mobility, greater conductance, and less influence of the Ba^{2+} Nernst potential on V_{rev}. However, under such circumstances, the bag cell neuron cation channel should display anomalous mol fraction, i.e. a smaller conductance in a Ca^{2+}–Ba^{2+} mix compared to either divalent ion alone (Hess and Tsien, 1984; Friel and Tsien, 1989). Our data indicate this is not the case, as the conductance in CaBaASW is essentially unchanged from nASW. In true Ca^{2+} channels, anomalous mol fraction is due to tightly bound Ca^{2+} repelling Ba^{2+}, making the latter less permeable provided there is extracellular Ca^{2+} present (Hess and Tsien, 1984; Hille, 2001). While other cation channels, such as TRPV5 and an *Aplysia* voltage-independent channel, do show anomalous mol fraction, they present much greater permeability to Ca^{2+} than other cations (Chesnoy-Marchais, 1985; Jean et al., 2002). Because the bag cell neuron cation channel is more non-selective, there may be adequate room for Ba^{2+} to permeate despite the repulsive presence of Ca^{2+}. As a case in point, the *Aplysia* nicotinic receptor cation channel is very non-selective for cations (Ascher et al., 1978). Moreover, not all Ca^{2+} permeable channels display anomalous mol fraction, e.g. ventricular myocyte voltage-dependent Ca^{2+} channels (Yue and Marban, 1990).

For a non-electrophysiological assessment of cation channel Ca^{2+} permeability, we used Mn^{2+} influx-induced fura quench in whole bag cell neurons (Hallam and Rink, 1985; Sage et al., 1989). The increased quench rate following activation by bath-applied CtVm is consistent with the cation channel passing Ca^{2+}. The constant quench of fura we observed at rest in the presence of Mn^{2+} alone is to be expected, as Ca^{2+} (i.e. Mn^{2+} in our conditions) continually leaks into both bag cell neurons and cells in general (Knox et al., 1996; Rizzuto and Pozzan, 2006; Friel and Chiel, 2008; Geiger et al., 2008). Other investigators have reported a similar decrease in fura isosbestic fluorescence with Mn^{2+} alone, which is in turn accelerated by the opening of Ca^{2+}-permeable cation channels or ionotropic receptors (Simpson et al., 1995; Brereton et al., 2001; Schaefer et al., 2002). It was necessary to image at the isosbestic wavelength, where fura is not sensitive to Ca^{2+} (Grynkiewicz et al., 1985), to avoid distortion of the results by any released intracellular Ca^{2+} (Magoski et al., 2000). Both pharmacological and biophysical evidence indicates that CtVm acts on membrane receptors to stimulate the cation channel through protein kinase C and Ca^{2+} release from the endoplasmic reticulum (Wilson and Kaczmarek, 1993; Magoski et al., 2002; Kachoei et al., 2004, 2006).

Regardless of extracellular Ca^{2+} concentration, the bag cell neuron cation channel shows inward rectification at voltages positive to -30 mV. This appears as a “flattening” of the I–V curve and results in two, distinct ranges of

from a mean of zero (one sample *t*-test). For this and subsequent bar graphs, the *n*-values are given within or just below a given bar. (C) *Left*, Voltage-clamp recordings show that CtVm (100 μg/ml; at arrow) produces prominent inward current consistent with cation channel opening (thick line), as compared to water (thin line). *Right*, Summary data demonstrate that CtVm induces a significantly larger peak current versus control (Mann–Whitney *U*-test). (D) *Left*, When compared to water (thin line), CtVm (thick line) causes a more rapid decline in the fura signal. The slower decline with water is likely due to a steady leak of Mn^{2+} into the neuron. *Right*, Summary data of the τ from single exponential fits show that fura is quenched at a significantly more rapid rate following CtVm application (Mann–Whitney *U*-test).

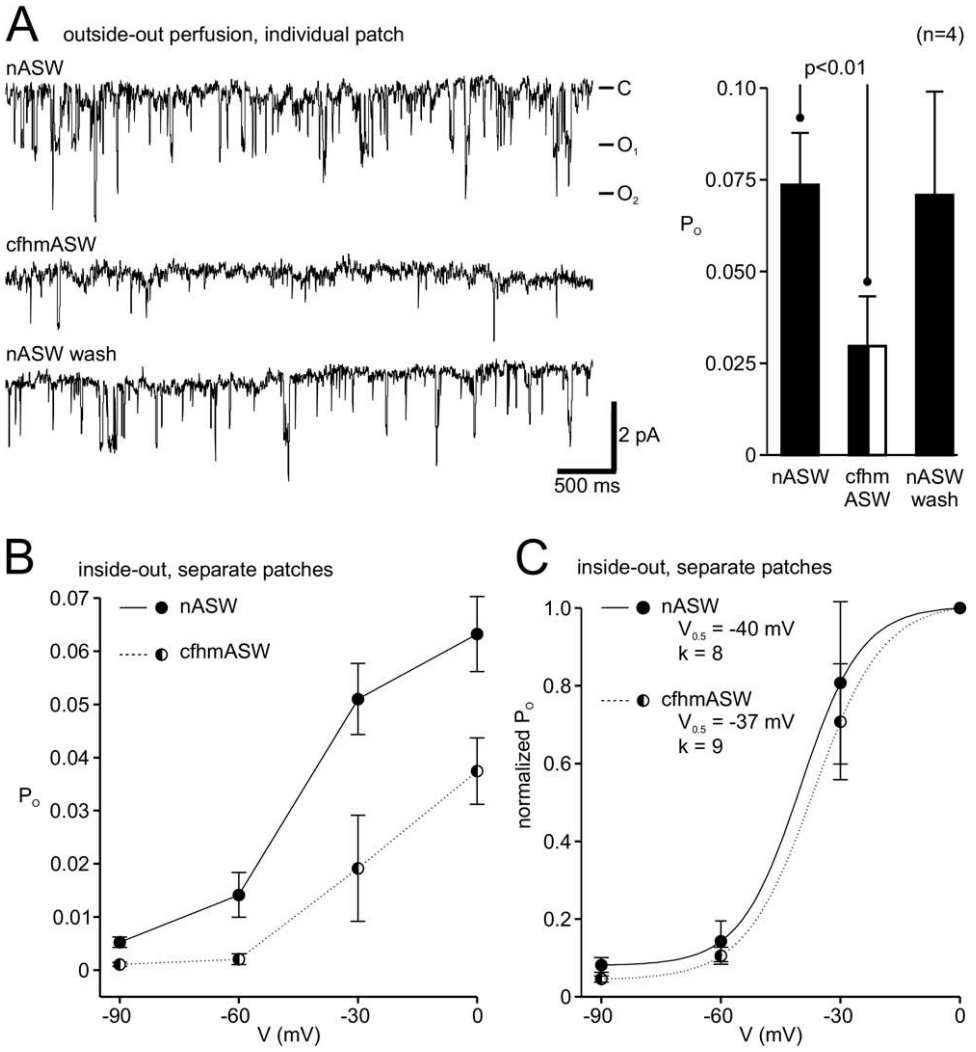

Fig. 6. Removal of extracellular Ca^{2+} lowers cation channel activity without changing voltage-dependence. (A) *Left*, An excised, outside-out patch voltage-clamped at −60 mV and containing two cation channels with nASW (11 mM Ca^{2+} and 55 mM Mg^{2+}) perfusing onto the extracellular face. Applying cfhmASW (0 mM Ca^{2+}, 66 mM Mg^{2+}) causes a obvious lowering of activity, which recovers upon return to nASW. *Right*, Summary data indicating that cfhmASW significantly reduces mean cation channel P_O when compared to nASW (paired Student's *t*-test). (B) P_O versus voltage curves for cation channels in excised, inside-out patches with nASW or cfhmASW at the extracellular face. These data represent separate patches and are taken from the experiment sets depicted in Figs. 1 and 2. Over the entire voltage range, the cation channels with nASW at the extracellular face have a greater P_O than those exposed to cfhmASW. (C) Single-channel activation curves (P_O normalized to P_O at 0 mV) in normal Ca^{2+} (closed circles, solid line; re-plotted from Fig. 1) or cfhmASW (half-closed circles, dotted line). A Boltzmann fit to the curves reveals that the $V_{0.5}$ and k are essentially the same in the presence or absence of extracellular Ca^{2+}.

current flow. The negative range (−90 to −30 mV) has greater conductance and overlaps with the membrane potential of the afterdischarge (−40 to −20 mV) (Kupfermann and Kandel, 1970; Kaczmarek et al., 1982). Thus, the channel will pass more current at those voltages where it is required to provide depolarizing drive. For certain cation channels, voltage-dependent intracellular Mg^{2+} block is responsible for inward rectification, and this is lessened or eliminated by Mg^{2+} removal (Inoue et al., 2001; Voets et al., 2003; Obukhov and Nowycky, 2005). However, the rectification of the bag cell neuron cation channel is not due to voltage-dependent block, as Mg^{2+}-free intracellular saline does not alter the I–V curve. More likely, rectification is intrinsic, which is in part the case for TRPV6 (Voets et al., 2003). That stated, our inside-out patch perfusion experiments do show that removing cytoplasmic face Mg^{2+} increases P_O without an obvious change in current amplitude, suggesting that Mg^{2+} is a slow blocker at −60 mV. A similar effect was reported for voltage-independent cation channels from the pond snail, *Lymnaea* (Strong and Scott, 1992). In bag cell neurons, intracellular Mg^{2+} may regulate the number of available cation channels at steady-state.

Ca^{2+}-activation of the bag cell neuron cation channel is achieved by closely-associated calmodulin (Lupinsky and Magoski, 2006). Our findings that P_O is decreased by either BaASW (Lupinsky and Magoski, 2006) or cfhmASW (present study) substantiate the conclusion that Ca^{2+} in-

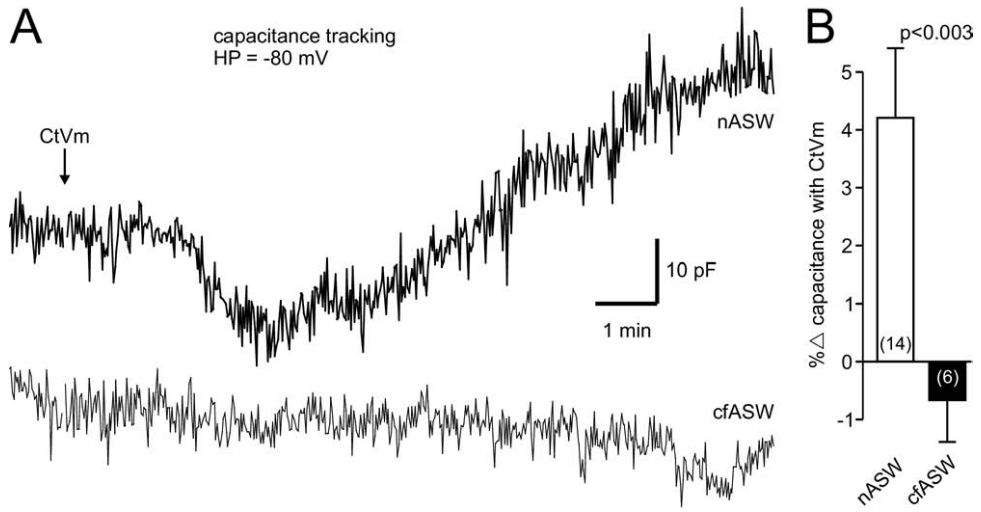

Fig. 7. Bag cell neuron membrane capacitance is increased by cation channel activation. (A) *Upper*, Under voltage-clamp at a holding potential (HP) of −80 mV, introduction of CtVm (100 μg/ml; at arrow) in nASW (11 mM Ca^{2+}; thick line) results in a transient reduction, followed by an elevation of capacitance. The short-lived drop in capacitance, before the subsequent increase, is present in 10 out of the 14 neurons recorded in nASW. *Lower*, In a different neuron, bathed in cfASW (0 mM Ca^{2+}; thin line), CtVm produces only a slow decline in capacitance. None of the neurons recorded in cfASW display the transient drop in capacitance. The scale bar applies to both traces. (B) Summary data demonstrate that CtVm induces a net increase in membrane capacitance that is significantly larger in nASW versus cfASW (paired Student's *t*-test). Means reflect peak changes in capacitance normalized to baseline.

flux provides positive feedback to the channel itself. As proposed for the TRPM2 cation channel (McHugh et al., 2003), the Ca^{2+} at the mouth of the pore that would normally bind channel-associated calmodulin is lost when replaced by Ba^{2+} or Mg^{2+}. Moreover, a lack of change to the single-channel activation curve with cfhmASW is consistent with reduced Ca^{2+}-dependent gating, rather than altered voltage-dependence, lowering P_O. The current study reveals that prior experiments of a similar nature with BaASW (Lupinsky and Magoski, 2006) held the caveat of voltage-dependence being prominently right-shifted by partial or complete replacement of extracellular Ca^{2+} with Ba^{2+}. Not surprisingly, foreign cations like Ba^{2+} or Sr^{2+} can alter the gating and voltage-dependence of other cation channels (Helliwell and Large, 1996; Albert and Large, 2001).

The bag cell neuron cation channel appears capable of causing secretion as assayed by capacitance tracking and CtVm application. We conclude that CtVm evokes cation channel–mediated Ca^{2+} influx-dependent secretion for several reasons. First, using capacitance tracking to detect vesicle fusion as changes in plasma membrane area is a well-established indirect measure of classic or peptide neurotransmitter release (Neher and Marty, 1982; Tse et al., 1997; Neves et al., 2001; Klyachko and Jackson, 2002). Second, at negative holding potentials CtVm opens the cation channel exclusively (Wilson et al., 1996). Only if the membrane potential is depolarized or left unclamped will CtVm recruit voltage-gated Ca^{2+} channels (Magoski et al., 2000). Third, when extracellular Ca^{2+} is removed, CtVm does not produce a change in capacitance. Fourth, although CtVm has been shown to evoke intracellular Ca^{2+} release (Magoski et al., 2000), a lack of secretion following CtVm in cfASW is consistent with both our laboratory and others demonstrating that depletion of Ca^{2+} from the endoplasmic reticulum fails to cause release (Jonas et al., 1997; Hickey et al., 2008). Parenthetically, for some neurons in nASW we did observe a temporary lowering of capacitance to CtVm, that presumably reflects an initial phase of endocytosis prior to exocytosis. The Ca^{2+} from the cation channel may not be as tightly coupled to the secretory pathway as that from voltage-gated Ca^{2+} channels, and thus has the potential to initiate membrane retrieval. For example, chromaffin cell endocytosis is enhanced by a general increase of intracellular Ca^{2+} (Engisch and Nowycky, 1998).

Although the Ca^{2+} flowing through the cation channel constitutes inward current during the afterdischarge, the bag cell neurons also take advantage of this biochemical signal. Magoski et al. (2000) suggested that cation channel–mediated Ca^{2+} entry is responsible for triggering the prolonged refractory period the bag cell neurons experience subsequent to an afterdischarge. The present data substantiate this concept to the extent that cation channel Ca^{2+} permeability appears genuine. A classic example of Ca^{2+} permeable cation channels initiating plasticity is the role of glutamate-gated *N*-methyl-D-aspartate (NMDA) receptors in LTP (Malenka and Nicoll, 1999). With respect to transmitter release, NMDA and purinergic channels can elicit secretion of 5-HT and norepinephrine, respectively, TRPC4 induces exocytosis from neuroendocrine cells, and an endogenous cation channel causes insulin release from a pancreatic cell line (Straub et al., 2000; Kim et al., 2004; Obukhov and Nowycky, 2002; De Kock et al., 2006). Thus, the bag cell neuron channel is one of a growing number of Ca^{2+} permeable cation channels that may participate in changing neuronal function or triggering secretion.

Acknowledgments—The authors thank Ms. S. L. Smith for excellent technical assistance, Ms. N. M. Magoski for critical evaluation of previous drafts of the manuscript, and the anonymous reviewers for providing constructive comments to improve the manuscript. C.M.H. holds an Ontario Graduate Scholarship in Science and Technology scholarship and N.S.M. holds a Canadian Institutes of Health Research (CIHR) New Investigator Award. Supported by CIHR operating grant to N.S.M.

REFERENCES

Aarts M, Iihara K, Wei W-L, Xiong Z-G, Arundine M, Cerwinski W, MacDonald JF, Tymianski M (2003) A key role for TRPM7 channels in anoxic neuronal death. Cell 115:863–877.

Albert AP, Large WA (2001) The effect of external divalent cations on spontaneous non-selective cation channel currents in rabbit portal vein myocytes. J Physiol 536:409–420.

Arch S (1972) Polypeptide secretion from the isolated parietovisceral ganglion of *Aplysia californica*. J Gen Physiol 59:47–59.

Ascher P, Marty A, Neild TO (1978) Life time and elementary conductance of the channels mediating the excitatory effects of acetylcholine in *Aplysia* neurones. J Physiol 278:177–206.

Brereton HM, Chen J, Rychkov G, Harland ML, Barritt GJ (2001) Maitotoxin activates an endogenous non-selective cation channel and is an effective initiator of the activation of the heterologously expressed hTRPC-1 (transient receptor potential) non-selective cation channel in H4-IIE liver cells. Biochim Biophys Acta Mol Cell Res 1540:107–126.

Chao S-H, Suzuki Y, Zysk JR, Cheung WY (1984) Activation of calmodulin by various metal cations as a function of ionic radius. Mol Pharmacol 26:75–82.

Chen QX, Perkins KL, Choi DW, Wong RKS (1997) Secondary activation of a cation conductance is responsible for NMDA toxicity in acutely isolated hippocampal neurons. J Neurosci 17:4032–4036.

Chesnoy-Marchais D (1985) Kinetic properties and selectivity of calcium-permeable single channels in *Aplysia* neurones. J Physiol 367:457–488.

Clapham DE (2003) TRP channels as cellular sensors. Nature 426:517–524.

Colquhoun D, Sigworth FJ (1995) Fitting and statistical analysis of single channel records. In: Single channel recording, 2nd ed (Sakmann B, Neher E, eds), pp 483–587. New York, NY: Plenum.

Congar P, Leinekugel X, Ben-Ari Y, Crepel V (1997) A long-lasting calcium-activated nonselective cationic current is generated by synaptic stimulation or exogenous activation of group 1 metabotropic glutamate receptors in CA1 pyramidal neurons. J Neurosci 17:5366–5379.

Cruz LJ, Corpuz G, Olivera BM (1976) A preliminary study of *Conus* venom protein. Veliger 18:302–308.

de Kock CPJ, Cornelisse LN, Burnashev N, Lodder JC, Timmerman AJ, Couey JJ, Mansvelder HD, Brussaard AB (2006) NMDA receptors trigger neurosecretion of 5-HT within dorsal raphe nucleus of the rat in the absence of action potential firing. J Physiol 577:891–905.

Dembrow NC, Jing J, Brezina V, Weiss KR (2004) A specific synaptic pathway activates a conditional plateau potential underlying protraction phase in the *Aplysia* feeding central pattern generator. J Neurosci 24:5230–5238.

DeRiemer SA, Schweitzer B, Kaczmarek LK (1985) Inhibitors of calcium-dependent enzymes prevent the onset of afterdischarge in the peptidergic bag cell neurons of *Aplysia*. Brain Res 340: 175–180.

Eckert R, Tillotson DL (1981) Calcium-mediated inactivation of the calcium conductance in caesium-loaded giant neurones of *Aplysia californica*. J Physiol 314:265–280.

Egorov AV, Hamam BN, Fransen E, Hasselmo ME, Alonso AA (2002) Graded persistent activity in entorhinal cortex neurons. Nature 420:173–178.

Engisch KL, Nowycky MC (1998) Compensatory and excess retrieval: two types of endocytosis following single step depolarizations in bovine adrenal chromaffin cells. J Physiol 506:591–608.

Fraser DD, MacVicar BA (1996) Cholinergic-dependent plateau potential in CA1 hippocampal pyramidal neurons. J Neurosci 16: 4113–4128.

Friel DD, Tsien RW (1989) Voltage-gated calcium channels: direct observation of the anomalous mole fraction effect at the single-channel level. Proc Natl Acad Sci U S A 86:5207–5211.

Friel DD, Chiel HJ (2008) Calcium dynamics: analyzing the Ca^{2+} regulatory network in intact cells. Trends Neurosci 31:8–19.

Gardam KE, Geiger JE, Hickey CM, Hung AY, Magoski NS (2008) Flufenamic acid affects multiple currents and causes intracellular Ca^{2+} release in *Aplysia* bag cell neurons. J Neurophysiol 100: 38–49.

Geiger JE, Magoski NS (2008) Ca^{2+}-induced Ca^{2+}-release in *Aplysia* bag cell neurons requires interaction between mitochondrial and endoplasmic reticulum stores. J Neurophysiol 100:24–37.

Gillis KD (1995) Techniques for membrane capacitance measurements. In: Single channel recording, 2nd ed (Sakmann B, Neher E, eds), pp 155–197. New York, NY: Plenum.

Grynkiewicz G, Poenie M, Tsien RY (1985) A new generation of calcium indicators with greatly improved fluorescent properties. J Biol Chem 260:3440–3448.

Hagiwara S, Fukuda J, Eaton DC (1974) Membrane currents carried by Ca, Sr, and Ba in barnacle muscle fiber during voltage clamp. J Gen Physiol 63:564–578.

Haiech J, Claude BBK, Demaille JJG (1981) Effects of cations on affinity of calmodulin for calcium: ordered binding of calcium ions allows for specific activation of calmodulin-stimulated enzymes. Biochemistry 20:3890–3897.

Haj-Dahmane S, Andrade R (1999) Muscarinic receptors regulate two different calcium-dependent nonselective cation currents in rat prefrontal cortex. Eur J Neurosci 11:1973–1980.

Hall BJ, Delaney KR (2002) Contribution of a calcium-activated nonspecific conductance to NMDA receptor-mediated synaptic potentials in granule cells of the frog olfactory bulb. J Physiol 543: 819–834.

Hallam TJ, Rink TJ (1985) Agonists stimulate divalent cation channels in the plasma membrane of human platelets. FEBS Lett 186: 175–179.

Helliwell RM, Large WA (1996) Dual effect of external Ca^{2+} on noradrenaline-activated cation current in rabbit portal vein smooth muscle cells. J Physiol 492:75–88.

Hermosura MC, Nayakanti H, Dorovkov MV, Calderon FR, Ryazanov AG, Haymer DS, Garruto RS (2005) A TRPM7 variant shows altered sensitivity to magnesium that may contribute to the pathogenesis of two Guamanian neurodegenerative disorders. Proc Natl Acad Sci U S A 102:11510–11515.

Hess P, Tsien RW (1984) Mechanism of ion permeation through calcium channels. Nature 309:453–456.

Hess P, Lansman JB, Tsien RW (1986) Calcium channel selectivity for divalent and monovalent cations. Voltage and concentration dependence of single channel current in ventricular heart cells. J Gen Physiol 88:293–319.

Hickey CM, Geiger JE, Magoski NS (2008) Calcium released from mitochondria depolarizes *Aplysia* bag cell neurons by activating a voltage-independent cation current. Soc Neurosci Abstr 34:12, 30.

Hille B (2001) Ionic channels of excitable membranes, 3rd ed. Sunderland, MA: Sinauer.

Hoth M (1995) Calcium and barium permeation through calcium release-activated calcium (CRAC) channels. Pflugers Arch 430: 315–322.

Hung AY, Magoski NS (2007) Activity-dependent initiation of a prolonged depolarization in *Aplysia* bag cell neurons: role for a cation channel. J Neurophysiol 97:2465–2479.

Inoue R, Okada T, Onoue H, Hara Y, Shimizu S, Naitoh S, Ito Y, Mori Y (2001) The transient receptor potential protein homologue TRP6

is the essential component of vascular 1-adrenoceptor-activated Ca^{2+}-permeable cation channel. Circul Res 88:325–332.

Jean K, Bernatchez G, Klein H, Garneau L, Sauvé R, Parent L (2002) Role of aspartate residues in Ca^{2+} affinity and permeation of the distal ECaC1. Am J Physiol Cell Physiol 282:C665–C672.

Jo K, Heien ML, Thompson LB, Zhong M, Nuzzo RG, Sweedler JV (2007) Mass spectrometric imaging of peptide release from neuronal cells within microfluidic devices. Lab Chip 7:1454–1460.

Jonas EA, Knox RJ, Smith TCM, Wayne NL, Connor JA, Kaczmarek LK (1997) Regulation by insulin of a unique neuronal Ca^{2+} pool and neuropeptide secretion. Nature 385:343–346.

Kachoei B, Imperial JS, Olivera BM, Magoski NS (2004) Actions of *Conus textile* venom on *Aplysia* bag cell neurons. Soc Neurosci Abstr 30:2, 86.

Kachoei BA, Lamb S, Magoski NS (2006) Protein kinase C plays a role in the initiation of bursting in *Aplysia* bag cell neurons. Soc Neurosci Abstr 32:6, 813.

Kaczmarek LK, Jennings KR, Strumwasser F (1978) Neurotransmitter modulation, phosphodiesterase inhibitor effects, and cyclic AMP correlates of afterdischarge in peptidergic neurites. Proc Natl Acad Sci U S A 75:5200–5204.

Kaczmarek LK, Jennings K, Strumwasser F (1982) An early sodium and a late calcium phase in the afterdischarge of peptide-secreting neurons of *Aplysia*. Brain Res 238:105–115.

Kaczmarek LK, Strumwasser F (1984) A voltage-clamp analysis of currents in isolated peptidergic neurons of *Aplysia*. J Neurophysiol 52:340–349.

Karai LJ, Russell JT, Iadarola MJ, Olah Z (2004) Vanilloid receptor 1 regulates multiple calcium compartments and contributes to Ca^{2+}-induced Ca^{2+} release in sensory neurons. J Biol Chem 279: 16377–16378.

Kim JH, Nam JH, Kim M-H, Koh D-S, Choi S-J, Kim SJ, Lee JE, Min KM, Uhm D-Y, Kim SJ (2004) Purinergic receptors coupled to intracellular Ca^{2+} signals and exocytosis in rat prostate neuroendocrine cells. J Biol Chem 279:27345–27356.

Kim SR, Lee DY, Chung ES, Oh UT, Kim SU, Jin BK (2005) Transient receptor potential vanilloid subtype 1 mediates cell death in mesencephalic dopamine neurons *in vivo* and *in vitro*. J Neurosci 25:662–671.

Klyachko VA, Jackson MB (2002) Capacitance steps and fusion pores of small and large-dense-core vesicles in nerve terminals. Nature 418:89–92.

Knox RJ, Jonas EA, Kao L-S, Smith PJS, Connor JA, Kaczmarek LK (1996) Ca^{2+} influx and activation of a cation current are coupled to intracellular Ca^{2+} release in peptidergic neurons of *Aplysia californica*. J Physiol 494:627–693.

Kramer RH, Zucker RS (1985) Calcium-dependent inward current in *Aplysia* bursting pace-maker neurones. J Physiol 362:107–130.

Kupfermann I (1967) Stimulation of egg laying: possible neuroendocrine function of bag cells of abdominal ganglion of *Aplysia californica*. Nature 216:814–815.

Kupfermann I (1970) Stimulation of egg laying by extracts of neuroendocrine cells (bag cells) of abdominal ganglion of *Aplysia*. J Neurophysiol 33:877–881.

Kupfermann I, Kandel ER (1970) Electrophysiological properties and functional interconnections of two symmetrical neurosecretory clusters (bag cells) in abdominal ganglion of *Aplysia*. J Neurophysiol 33:865–876.

Lim NF, Nowycky MC, Bookman RJ (1990) Direct measurement of exocytosis and calcium currents in single vertebrate nerve terminals. Nature 344:449–451.

Loechner KJ, Azhderian EM, Dreyer R, Kaczmarek LK (1990) Progressive potentiation of peptide release during a neuronal discharge. J Neurophysiol 63:738–744.

Lu B, Su Y, Das S, Wang H, Wang Y, Liu J, Ren D (2009) Peptide neurotransmitters activate a cation channel complex of NALCN and UNC-80. Nature 457:741–744.

Lupinsky DA, Magoski NS (2006) Ca^{2+}-dependent regulation of a non-selective cation channel from *Aplysia* bag cell neurones. J Physiol 575:491–506.

Magoski NS, Knox RJ, Kaczmarek LK (2000) Activation of a Ca^{2+}-permeable cation channel produces a prolonged attenuation of intracellular Ca^{2+} release in *Aplysia* bag cell neurons. J Physiol 522:271–283.

Magoski NS, Wilson GF, Kaczmarek LK (2002) Protein kinase modulation of a neuronal cation channel requires protein–protein interaction mediated by an Src homology 3 domain. J Neurosci 22:1–9.

Magoski NS (2004) Regulation of an *Aplysia* bag cell neuron cation channel by closely associated protein kinase A and a protein phosphatase. J Neurosci 24:6833–6841.

Magoski NS, Kaczmarek LK (2004) Protein kinases and neuronal excitability. In: Encyclopedia of neuroscience, 3rd ed [CD-ROM] (Adelman G, Smith BH, eds). New York, NY: Elsevier.

Magoski NS, Kaczmarek LK (2005) Association/dissociation of a channel-kinase complex underlies state-dependent modulation. J Neurosci 25:8037–8047.

Malenka RC, Nicoll RA (1999) Long-term potentiation—a decade of progress? Science 285:1870–1874.

McHugh D, Flemming R, Xu S-Z, Perraud A-L, Beech DJ (2003) Critical intracellular Ca^{2+} dependence of transient receptor potential melastatin 2 (TRPM2) cation channel activation. J Biol Chem 278:11002–11006.

Mermelstein PG, Deisseroth K, Dasgupta N, Isaksen AL, Tsien RW (2001) Calmodulin priming: nuclear translocation of a calmodulin complex and the memory of prior neuronal activity. Proc Natl Acad Sci U S A 98:15342–15347.

Michel S, Wayne NL (2002) Neurohormone secretion persists after post-afterdischarge membrane depolarization and cytosolic calcium elevation in peptidergic neurons in intact nervous tissue. J Neurosci 22:9063–9069.

Morisset V, Nagy F (1999) Ionic basis for plateau potentials in deep dorsal horn neurons of the rat spinal cord. J Neurosci 19:7309–7316.

Munsch T, Freichel M, Flockerzi V, Pape H-C (2003) Contribution of transient receptor potential channels to the control of GABA release from dendrites. Proc Natl Acad Sci U S A 100:16065–16070.

Neher E, Marty A (1982) Discrete changes of cell membrane capacitance observed under conditions of enhanced secretion in bovine adrenal chromaffin cells. Proc Natl Acad Sci U S A 79:6712–6716.

Neher E, Sakaba T (2008) Multiple roles of calcium ions in the regulation of neurotransmitter release. Neuron 59:861–872.

Neves G, Gomis A, Lagnado L (2001) Calcium influx selects the fast mode of endocytosis in the synaptic terminal of retinal bipolar cells. Proc Natl Acad Sci U S A 98:15282–15287.

Obukhov AG, Nowycky MC (2002) TRPC4 can be activated by G-protein-coupled receptors and provides sufficient Ca^{2+} to trigger exocytosis in neuroendocrine cells. J Biol Chem 277:16172–16178.

Obukhov AG, Nowycky MC (2005) A cytosolic residue mediates Mg^{2+} block and regulates inward current amplitude of a transient receptor potential channel. J Neurosci 25:1234–1239.

Ozawa T, Sasaki K, Umezawa Y (1999) Metal ion selectivity for formation of the calmodulin-metal-target peptide ternary complex studied by surface plasmon resonance spectroscopy. Biochim Biophys Acta 1434:211–220.

Partridge LD, Swandulla D (1988) Ca^{2+}-activated non-specific cation channels. Trends Neurosci 11:69–72.

Partridge LD, Muller TH, Swandulla D (1994) Calcium-activated non-selective channels in the nervous system. Brain Res Rev 19: 310–325.

Perrier J-F, Hounsgaard J (2003) 5-HT_2 receptors promote plateau potentials in turtle spinal motoneurons by facilitating an L-type calcium current. J Neurophysiol 89:954–959.

Pinsker HM, Dudek FE (1977) Bag cell control of egg laying in freely behaving *Aplysia*. Science 197:490–493.

Putzier I, Kullmann PHM, Horn JP, Levitan ES (2009) Dopamine neuron responses depend exponentially on pacemaker interval. J Neurophysiol 101:926–933.

Raman IM, Gustafson AE, Padgett D (2000) Ionic currents and spontaneous firing in neurons isolated from the cerebellar nuclei. J Neurosci 20:9004–9016.

Rizzuto R, Pozzan T (2006) Microdomains of intracellular Ca^{2+}: molecular determinants and functional consequences. Physiol Rev 86:369–408.

Rothman BS, Weir G, Dudek FE (1983) Egg-laying hormone: direct action on the ovotestis of *Aplysia*. Gen Comp Endocrinol 52: 134–141.

Sage SO, Merritt JE, Hallam TJ, Rink TJ (1989) Receptor-mediated calcium entry in fura-2-loaded human platelets stimulated with ADP and thrombin. Dual-wavelengths studies with Mn^{2+}. Biochem J 258:923–926.

Schaefer M, Plant TD, Stresow N, Albrecht N, Schultz G (2002) Functional differences between TRPC4 splice variants. J Biol Chem 277:3752–3759.

Siemens J, Zhou S, Piskorowski R, Nikai T, Lumpkin EA, Basbaum AI, King D, Julius D (2006) Spider toxins activate the capsaicin receptor to produce inflammatory pain. Nature 444:208–212.

Simpson PB, Challiss RAJ, Nahorski SR (1995) Divalent cation entry in cultured rat cerebellar granule cells measured using Mn^{2+} quench of fura 2 fluorescence. Eur J Neurosci 7:831–840.

Straub SG, Kornreich B, Oswald RE, Nemeth EF, Sharp GWG (2000) The calcimimetic R-467 potentiates insulin secretion in pancreatic cells by activation of a nonspecific cation channel. J Biol Chem 275:18777–18784.

Strong JA, Scott SA (1992) Divalent-selective voltage-independent calcium channels in *lymnaea* neurons: permeation properties and inhibition by intracellular magnesium. J Neurosci 12:2993–3003.

Strubing C, Krapivinsky G, Krapivinsky L, Clapham DE (2001) TRPC1 and TRPC5 form a novel cation channel in mammalian brain. Neuron 29:645–655.

Tahvildari B, Alonso AA, Bourque CW (2008) Ionic basis of ON and OFF persistent activity in layer III lateral entorhinal cortical principal neurons. J Neurophysiol 99:2006–2011.

Tam AKT, Magoski NS (2007) A persistent, voltage-dependent calcium current in neuroendocrine cells. Can J Neurol Sci 34(Suppl 3):326.

Tillotson D (1979) Inactivation of Ca^{2+} conductance dependent on entry of Ca^{2+} ions in molluscan neurons. Proc Natl Acad Sci U S A 76:1497–1500.

Tse FW, Tse A, Hille B, Horstmann H, Almers W (1997) Local Ca^{2+} release from internal stores controls exocytosis in pituitary gonadotrophs. Neuron 18:121–132.

Voets T, Janssens A, Prenen J, Droogmans G, Nilius B (2003) Mg^{2+}-dependent gating and strong inward rectification of the cation channel TRPV6. J Gen Physiol 121:245–260.

Vorndran C, Minta A, Poenie M (1995) New fluorescent calcium indicators designed for cytosolic retention or measuring calcium near membranes. Biophys J 69:2112–2124.

Wang C-LA (1985) A note on Ca^{2+} binding to calmodulin. Biochem Biophys Res Commun 130:426–430.

Wang GX, Poo M-M (2005) Requirement of TRPC channels in netrin-1-induced chemotropic turning of nerve growth cones. Nature 434:898–904.

Wilson GF, Kaczmarek LK (1993) Mode-switching of a voltage-gated cation channel is mediated by a protein kinase A-regulated tyrosine phosphatase. Nature 366:433–438.

Wilson GF, Richardson FC, Fisher TE, Olivera BM, Kaczmarek LK (1996) Identification and characterization of a Ca^{2+}-sensitive nonspecific cation channel underlying prolonged repetitive firing in *Aplysia* neurons. J Neurosci 16:3661–3671.

Wilson GF, Magoski NS, Kaczmarek LK (1998) Modulation of a calcium-sensitive nonspecific cation channel by closely associated protein kinase and phosphatase activities. Proc Natl Acad Sci U S A 95:10938–10943.

Yellen G (1982) Single Ca^{2+}-activated nonselective cation channels in neuroblastoma. Nature 296:357–359.

Yu X, Duan K-L, Shang C-F, Yu H-G, Zhou Z (2004) Calcium influx through hyperpolarization-activated cation channels (I_h channels) contributes to activity-evoked neuronal secretion. Proc Natl Acad Sci U S A 101:1051–1056.

Yue DT, Marban E (1990) Permeation in the dihydropyridine-sensitive calcium channel. Multi-ion occupancy but no anomalous mole-fraction effect between Ba^{2+} and Ca^{2+}. J Gen Physiol 95:911–939.

Zhang B, Wootton JF, Harris-Warrick RM (1995) Calcium-dependent plateau potentials in a crab stomatograstric ganglion motor neuron. II. Calcium-activated slow inward current. J Neurophysiol 74: 1938–1946.

Zhang C, Roepke TA, Kelly MJ, Ronnekleiv OK (2008) Kisspeptin depolarizes gonadotropin-releasing hormone neurons through activation of TRPC-like cationic channels. J Neurosci 28:4423–4434.

Zuhlke RD, Pitt GS, Deisseroth K, Tsien RW, Reuter H (1999) Calmodulin supports both inactivation and facilitation of L-type calcium channels. Nature 399:159–162.

(Accepted 5 May 2009)
(Available online 7 May 2009)